

UCLA

UCLA Previously Published Works

Title

CCL21-DC in situ vaccination in murine NSCLC overcomes resistance to immunotherapy and generates systemic tumor-specific immunity

Permalink

<https://escholarship.org/uc/item/2sf2b20q>

Journal

Journal for ImmunoTherapy of Cancer, 11(9)

ISSN

2051-1426

Authors

Salehi-Rad, Ramin

Lim, Raymond J

Du, Yushen

et al.

Publication Date

2023-09-01

DOI





10.1136/jitc-2023-006896

Copyright Information

This work is made available under the terms of a Creative Commons Attribution-NonCommercial License, available at <https://creativecommons.org/licenses/by-nc/4.0/>

Peer reviewed

CCL21-DC in situ vaccination in murine NSCLC overcomes resistance to immunotherapy and generates systemic tumor-specific immunity

Ramin Salehi-Rad ^{1,2}, Raymond J Lim,³ Yushen Du,^{3,4} Linh M Tran,^{1,2} Rui Li ¹, Stephanie L Ong,¹ Zi Ling Huang,¹ Camelia Dumitras,¹ Tianhao Zhang,³ Stacy J Park,¹ William Crosson,³ Bitta Kahangi,¹ Jensen Abascal,¹ Christopher Seet,¹ Michael Oh,¹ Maryam Shabihkhani,⁵ Manash Paul ¹, Kostyantyn Krysan,¹ Aaron E Lisberg,¹ Edward B Garon ¹, Bin Liu,¹ Steven M Dubinett^{1,2}

To cite: Salehi-Rad R, Lim RJ, Du Y, *et al.* CCL21-DC in situ vaccination in murine NSCLC overcomes resistance to immunotherapy and generates systemic tumor-specific immunity. *Journal for ImmunoTherapy of Cancer* 2023;0:e006896. doi:10.1136/jitc-2023-006896

► Additional supplemental material is published online only. To view, please visit the journal online (<http://dx.doi.org/10.1136/jitc-2023-006896>).

RS-R and RJL contributed equally.

Accepted 16 July 2023



© Author(s) (or their employer(s)) 2023. Re-use permitted under CC BY-NC. No commercial re-use. See rights and permissions. Published by BMJ.

For numbered affiliations see end of article.

Correspondence to

Dr Steven M Dubinett;
sdubinett@mednet.ucla.edu

Mrs Bin Liu;
bliu@mednet.ucla.edu

ABSTRACT

Background Despite recent advances in immunotherapy, many patients with non-small cell lung cancer (NSCLC) do not respond to immune checkpoint inhibitors (ICI). Resistance to ICI may be driven by suboptimal priming of antitumor T lymphocytes due to poor antigen presentation as well as their exclusion and impairment by the immunosuppressive tumor microenvironment (TME). In a recent phase I trial in patients with NSCLC, in situ vaccination (ISV) with dendritic cells engineered to secrete CCL21 (CCL21-DC), a chemokine that facilitates the recruitment of T cells and DC, promoted T lymphocyte tumor infiltration and PD-L1 upregulation.

Methods Murine models of NSCLC with distinct driver mutations (*Kras*^{G12D}/*P53*^{+/-}/*Lkb1*^{+/-} (KPL); *Kras*^{G12D}/*P53*^{+/-} (KP); and *Kras*^{G12D} (K)) and varying tumor mutational burden were used to evaluate the efficacy of combination therapy with CCL21-DC ISV plus ICI. Comprehensive analyses of longitudinal preclinical samples by flow cytometry, single cell RNA-sequencing (scRNA-seq) and whole-exome sequencing were performed to assess mechanisms of combination therapy.

Results ISV with CCL21-DC sensitized immune-resistant murine NSCLCs to ICI and led to the establishment of tumor-specific immune memory. Immunophenotyping revealed that CCL21-DC obliterated tumor-promoting neutrophils, promoted sustained infiltration of CD8 cytolytic and CD4 Th1 lymphocytes and enriched progenitor T cells in the TME. Addition of ICI to CCL21-DC further enhanced the expansion and effector function of T cells both locally and systemically. Longitudinal evaluation of tumor mutation profiles revealed that CCL21-DC plus ICI induced immunoediting of tumor subclones, consistent with the broadening of tumor-specific T cell responses.

Conclusions CCL21-DC ISV synergizes with anti-PD-1 to eradicate murine NSCLC. Our data support the clinical application of CCL21-DC ISV in combination with checkpoint inhibition for patients with NSCLC.

BACKGROUND

Lung cancer is the leading cause of cancer-related death worldwide and non-small cell lung cancer (NSCLC) is the most prevalent

WHAT IS ALREADY KNOWN ON THIS TOPIC

⇒ Poor antigen presentation in conjunction with an immunosuppressive tumor microenvironment attenuate host T cell responses and drive resistance to immunotherapy in patients with advanced non-small cell lung cancer (NSCLC).

WHAT THIS STUDY ADDS

⇒ CCL21-dendritic cell in situ vaccination combined with anti-PD-1 expands the functional repertoire of tumor-specific T cells and provides synergistic anti-tumor efficacy in resistant murine models of NSCLC.

HOW THIS STUDY MIGHT AFFECT RESEARCH, PRACTICE OR POLICY

⇒ These studies support the clinical evaluation of this combination immunotherapy in patients with NSCLC who are refractory to front-line therapy.

histological subtype.^{1 2} Recent advances in immunotherapy with immune checkpoint inhibitors (ICIs) that target the programmed death-1 (PD-1)/programmed death-ligand 1 (PD-L1) axis have revolutionized the treatment landscape of NSCLC. ICIs targeting the PD-1/PD-L1 pathway are now front-line therapy for most patients with advanced-stage NSCLC, either as monotherapy for PD-L1 high tumors or in combination with chemotherapy.^{3–5} However, many patients fail to respond to ICIs or acquire resistance after an initial response.⁶

Favorable responses to PD-1/PD-L1 blockade have been associated with high tumor mutational burden (TMB), increased baseline PD-L1 expression and CD8 T lymphocyte infiltration in the tumor microenvironment (TME).^{7–10} Clonal TMB and a

dormant tumor-infiltrating lymphocyte (TIL) phenotype as well as elevated *C-X-C motif chemokine ligand 9 (CXCL9)* expression and an interferon gamma (IFN- γ) gene signature in the TME have also been associated with improved clinical benefit of ICI.^{11–14} In contrast, impaired tumor antigen presentation has been correlated with resistance to ICI.^{6 15 16} These biomarkers of response that are intimately connected to the host adaptive immune axis highlight the pivotal role of antigen-reactive T lymphocytes in mediating antitumor responses to ICI.¹⁷ Therapies that enhance the quality and breadth of host tumor-specific T cell responses hold promise for combating immune resistance and evasion in NSCLC.

One approach to enhance host tumor-specific T cell responses and augment the efficacy of ICI in NSCLC is to use in situ vaccination (ISV) with autologous dendritic cells (DC), which are professional antigen presenting cells that mediate T cell activation.^{18–20} This antigen-agnostic approach provides DCs access to the entire repertoire of tumor antigens and can potentially generate broad antigen-specific T cell responses. In preclinical trials, we and others have shown that ISV with gene-modified bone marrow-derived DCs (BM-DCs) that secrete C-C Motif Chemokine Ligand 21 (CCL21) elicit potent antitumor immunity, which is dependent on CD8 T lymphocytes as well as the IFN- γ inducible chemokines, CXCL9 and C-X-C motif chemokine ligand 10 (CXCL10).^{21–23} CCL21 is a chemokine of interest for DC ISV because it facilitates T cell activation by promoting colocalization of naïve lymphocytes and antigen-experienced DCs.²⁴ In multiple preclinical studies, ISV with CCL21-DC demonstrated superior antitumor efficacy and enhanced capacity to induce influx of endogenous T cells into the tumor compared with mock-transduced DC (mock-DC), recombinant CCL21, and fibroblast secreting CCL21.^{22 23} These data highlight the critical contribution of both DCs and the CCL21 chemokine for the generation of effective vaccine-mediated antitumor immune responses. In a phase I clinical trial, we have shown the feasibility and safety of this ISV approach by intratumoral (IT) administration of autologous CCL21-DC, derived from peripheral blood monocytes, in patients with advanced stage NSCLC.²⁵ ISV with CCL21-DC increased CD8 T cell infiltration into the tumor and induced systemic tumor-specific immune responses in a subset of patients.²⁵ A concurrent upregulation of PD-L1 in the TME was observed following CCL21-DC ISV, which may lead to T cell exhaustion and dysfunction. We hypothesized that CCL21-DC ISV in combination with anti-PD-1 could result in effective and durable tumor-specific T cell responses and potentially sensitize immune resistant NSCLC to ICI.

Here, we used murine models of oncogene-driven NSCLC with varying TMB that are resistant to anti-PD-1 monotherapy and found that CCL21-DC ISV synergizes with anti-PD-1 immunotherapy, inducing T cell activation, leading to enhanced antitumor efficacy as well as systemic tumor-specific immune memory. These studies support the clinical translation of CCL21-DC ISV in combination

with PD-1 blockade as a novel strategy to overcome resistance to immunotherapy in NSCLC.

RESULTS

CCL21-DC ISV potentiates the efficacy of anti-PD-1 in murine NSCLC models

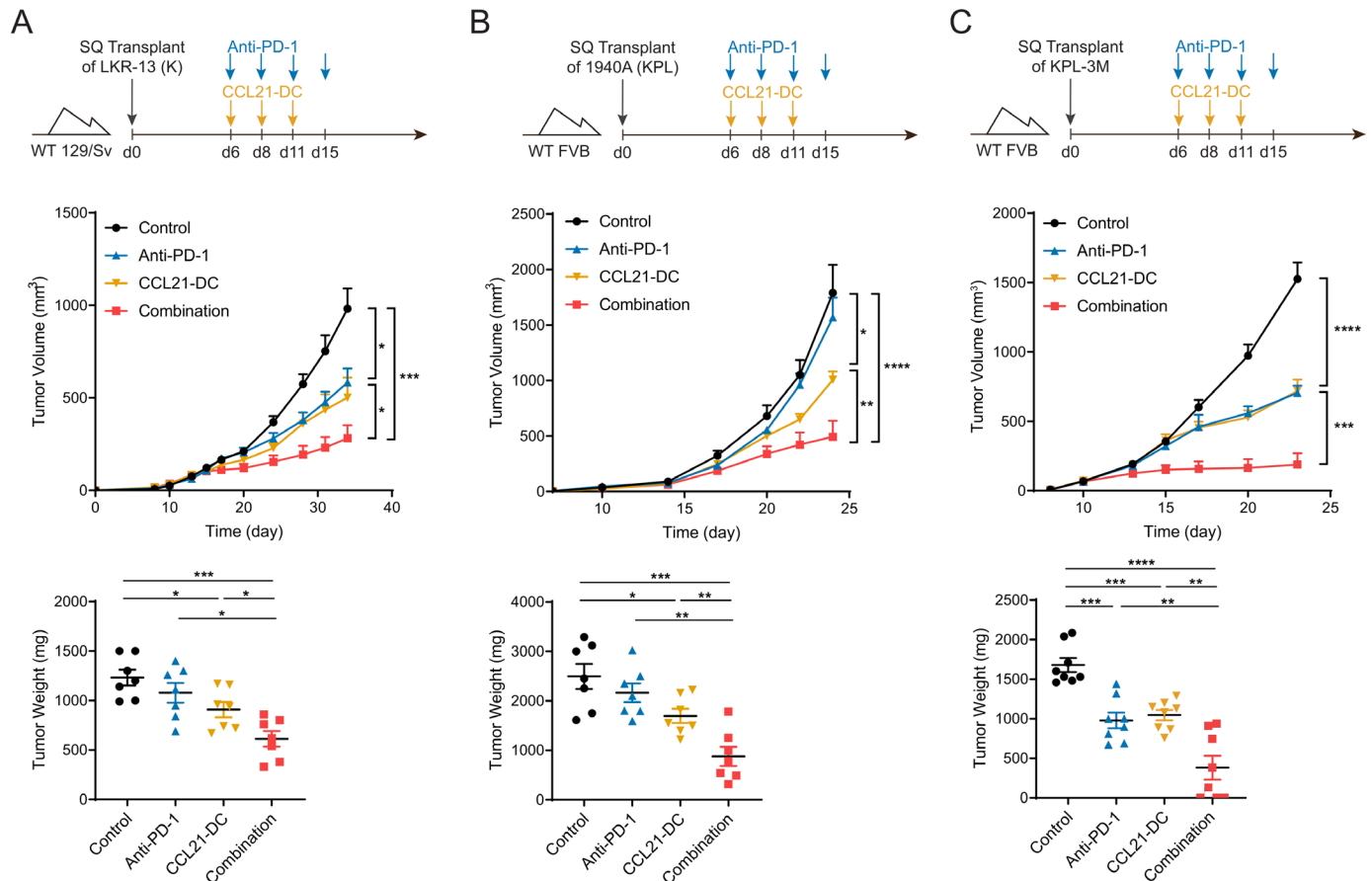
The efficacy of IT CCL21-DC in combination with anti-PD-1 was evaluated in multiple syngeneic murine models of NSCLC. CCL21-DCs were generated from murine BM²² and characterized as described in online supplemental materials and methods and Fig. S1A–E. Immunocompetent mice bearing LKR-13 tumors (a NSCLC cell line established from a *K-ras*^{LA1} mouse²⁶) were treated with IT CCL21-DC or intraperitoneal (IP) anti-PD-1 monotherapy or a combination of CCL21-DC and anti-PD-1 (figure 1A). While CCL21-DC and anti-PD-1 monotherapies generated modest antitumor efficacy, the combination therapy resulted in a significant reduction of tumor growth. Combination therapy with IT CCL21-DC and IP anti-PD-1 was also evaluated in mice bearing *Kras*-mutant tumors with co-occurring inactivating mutations of *Lkb1*, which has been identified as the major genetic driver of primary resistance to anti-PD-1 therapy.²⁷ As anticipated, mice-bearing 1940A murine tumors (a NSCLC cell line established from a conditional *Kras*^{G12D}*T-p53*^{+/-}*Lkb1*^{-/-}*Luc* (KPL) mouse²⁶) were resistant to anti-PD-1, while IT CCL21-DC monotherapy showed minor reduction of tumor growth, but combination of anti-PD-1 and IT CCL21-DC significantly inhibited tumor growth (figure 1B).

CCL21-DC ISV plus anti-PD-1 synergistically inhibit tumor growth in a LKB1-deficient murine model of NSCLC with high TMB

In contrast to human NSCLC, genetically engineered murine models of NSCLC harbor low TMB with few protein-altering mutations.²⁸ Specifically, the LKR-13 and 1940A tumors possess 0.67 and 1.75 mutations per Mb, respectively.²⁶ Because the antitumor efficacy of the combination immunotherapy could potentially be limited by the paucity of tumor neoantigens in these models, we evaluated the efficacy of IT CCL21-DC and anti-PD-1 in the KPL-3M syngeneic model with increased TMB (7.2 mutations per Mb) that closely approximates the TMB of human NSCLC.²⁶ In accord with our previous findings, IT CCL21-DC and anti-PD-1 monotherapies elicited moderate antitumor efficacy in the KPL-3M model, whereas the combination therapy resulted in a synergistic antitumor response with eradication of approximately 40% of tumors (figure 1C, online supplemental figure S1F).

CCL21-DC ISV and anti-PD-1 as monotherapies or in combination reprogram tumor-infiltrating neutrophils to an antitumor phenotype

To evaluate the immune determinants of synergistic antitumor responses in KPL-3M tumor-bearing mice following CCL21-DC ISV and anti-PD-1 combination therapy, the



immune components of the TME were profiled by single cell RNA sequencing (scRNA-seq) on day 15 (figure 2A). Flow phenotyping of the same tumors and associated tumor-draining lymph nodes (TdLNs) was also performed (figure 2A and online supplemental figure S2A). These studies were performed on day 15, 9 days following the initiation of treatment, to provide sufficient time for the activation of host adaptive immune responses without significant changes in tumor size among different groups (online supplemental figure S2B). Combination therapy resulted in a substantial enrichment of CD45⁺ leucocytes in the TME compared with control or CCL21-DC and anti-PD-1 monotherapies as determined by flow cytometry (online supplemental figure S2C).

The scRNA-seq analysis of the CD45⁺ population within the TME revealed five immune clusters based on expression profiles of known lineage marker genes, corresponding to neutrophil, monocyte (Mono)/macrophage (MΦ)/DC, plasmacytoid DC, NK/T cells and B cells (figure 2B,C). Neutrophils were the most abundant immune population within the CD45⁺ compartment

of the KPL-3M tumors, consistent with prior reports revealing a neutrophil-enriched TME in LKB1-deficient NSCLC^{27–29} (figure 2C). Clustering of neutrophils in KPL-3M tumors identified four subsets (clusters C1–C4) (figure 2D). A recent single-cell analysis of murine and human lung cancers identified six conserved neutrophil subsets (N1–N6).³⁰ Tumor-infiltrating neutrophils (TIN) formed a continuum of states, where N1 neutrophils present in healthy tissue with high expressions of canonical neutrophil markers, progressed continuously in the TME via N3 and N4 states to N5 neutrophils with tumor-promoting phenotypes defined by *Ccl3*, *Cd63*, *Cstb*, and *Ctsb* expression.³⁰ An N2 neutrophil subtype with a strong transcriptional signature of type I IFN response genes, apart from the continuum of states, was also observed, predominantly in healthy tissue. Using these reference datasets,³⁰ we defined C1 as N2 and C4 as N5. C2 shared the gene expression signature of closely related N4 and N6 subsets, and the transcriptome of C3 resembled the gene expression profiles of N1 and N3 (figure 2E). Treatment with CCL21-DC and anti-PD-1 combination

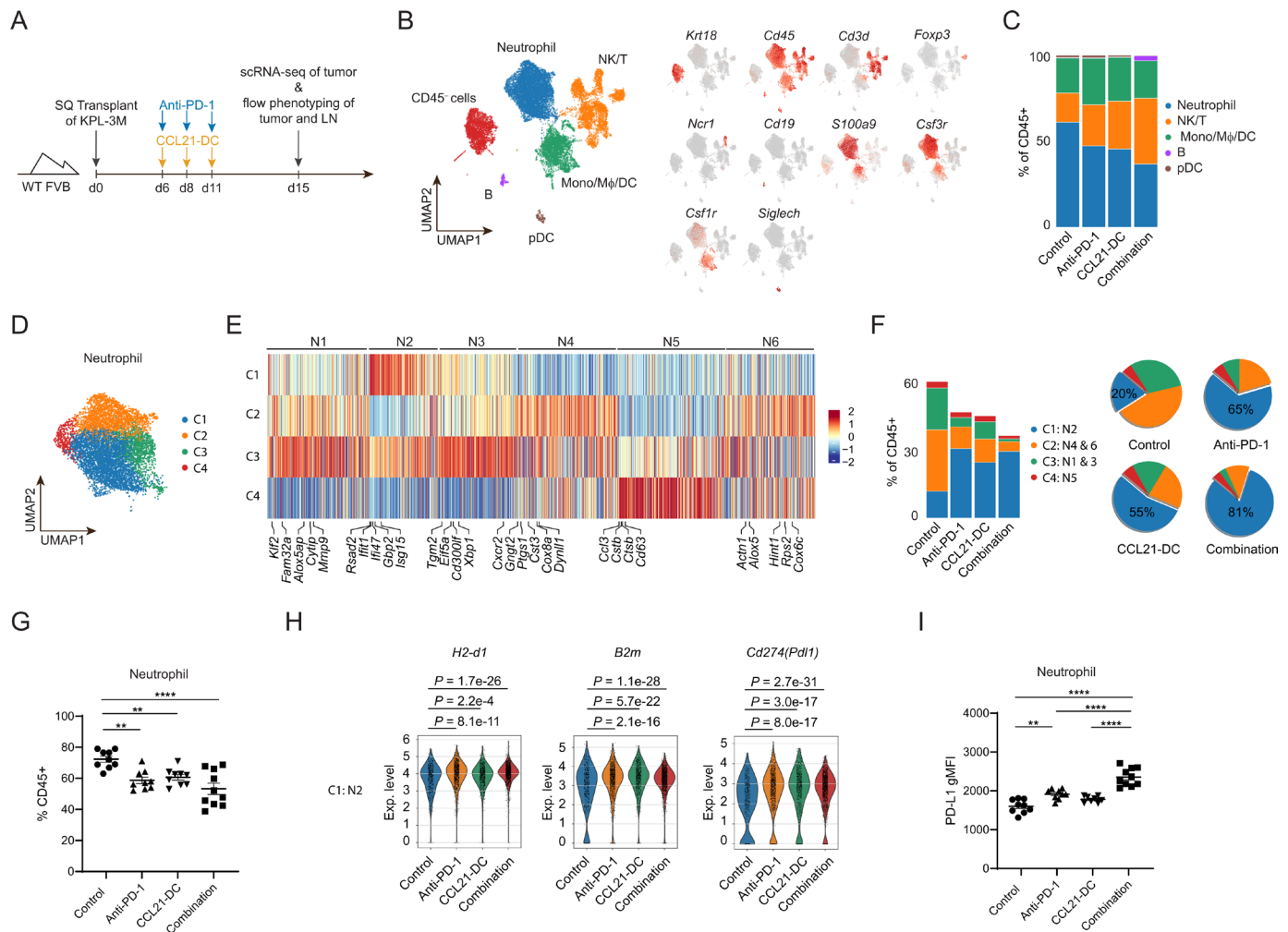


Figure 2 CCL21-DC ISV and anti-PD-1 as monotherapies or in combination suppress tumor-promoting neutrophils and induce antitumor neutrophils in the TME. (A) FVB mice were injected subcutaneously with 1.5×10^5 KPL-3M cells on day 0 (d0) and tumors were treated with vehicle control, 1.0×10^6 CCL21-DC, 200 μ g of anti-PD-1, or combination as indicated in the scheme. Tumor and TdLN were harvested on day 15 for immunophenotyping by flow cytometry ($n=6-10$ per group) and scRNA-seq (six tumors pooled per group). (B) UMAP plot of major immune clusters in the TME. (C) Frequency of different immune populations within CD45⁺ cells by scRNA-seq. (D) UMAP plot visualizing four subclusters within the neutrophil population. (E) Heatmap showing differential expression of referenced genes from neutrophil subsets (N1–N6) across C1–C4. (F) Frequency of neutrophil clusters (C1:N2, C2:N4&6, C3:N1&3, C4:N5) within CD45⁺ cells by scRNA-seq shown as bar graph (left), or distribution of each subcluster within the neutrophil population as pie chart (right). (G) Frequency of neutrophils within CD45⁺ cells by flow cytometry. (H) Violin plots illustrating the differential expression of designated genes in the C1:N2 neutrophil subset among different treatment groups. (I) Geometric mean fluorescence intensity (gMFI) of PD-L1 on neutrophils as determined by flow cytometry. Flow cytometry results are representative of two biological replicates of 6–10 mice per group. scRNA-seq was performed once. P values were determined by unpaired t-test. ** $p < 0.01$, **** $p < 0.0001$. DC, dendritic cell; ISV, in situ vaccination; TdLN, tumor-draining lymph node; TME, tumor microenvironment; UMAP, Uniform Manifold Approximation and Projection.

therapy resulted in the reduction of TINs in the CD45⁺ compartment as determined by scRNA-seq and flow cytometry (figure 2F,G). Significant enrichment of the C1 (N2) subset with an expression signature of type I IFN response and a concurrent reduction of C2 (tumor-associated N4 and N6) and C3 (canonical N1 and tumor-specific N3) clusters were noted in mice treated with anti-PD-1, CCL21-DC, or combination therapy compared with control, with the most substantial changes observed with the combination therapy (figure 2F). Increased expression of IFN- γ downstream genes, including *H2-d1* and *B2m* (encoding the antigen-presenting genes) and

the checkpoint inhibitor *Cd274* (encoding PD-L1), was also noted broadly across all TIN clusters following treatments (figure 2H and online supplemental figure S2D), suggesting immune activation in the TME. Increased PD-L1 surface protein expression by TINs was confirmed by flow cytometry with the highest magnitude observed with the CCL21-DC and anti-PD-1 combination therapy (figure 2I). These results demonstrate that CCL21-DC and anti-PD-1 as monotherapies or in combination profoundly alter the composition and gene expression of the neutrophil compartment within the TME, resulting in an enrichment of the C1 (N2) neutrophil population

with a type I IFN response gene signature and a reduction of tumor-promoting neutrophil subtypes as well as increased expression of IFN downstream genes among all neutrophil subpopulations.

CCL21-DC alone or in combination with anti-PD-1 promotes the enrichment of activated mregDC in the TME and the migration of endogenous conventional DC1/conventional DC2 to TdLN

The tumor-infiltrating Mono/Mφ/DC population, characterized by scRNA-seq, contained four clusters (C1–C4) which were annotated based on known reference gene sets.^{30–31} C3 was identified as DC based on the high expression of canonical DC markers, including *Flt3*, *Zbtb46*, and *Dpp4* (online supplemental figure S3A–C). Tumor-infiltrating DCs are a heterogeneous group of cells with conserved signatures across cancer types in human and mouse.³² Conventional DCs (cDC) are comprised of two subtypes, cDC1 and cDC2. cDC1s, which develop under the influence of basic leucine zipper ATF-like transcription factor 3 (BATF3) and interferon regulatory factor 8 (IRF-8), specialize in antigen cross-presentation and CD8 T cell activation, whereas cDC2s may be more relevant for CD4 T cell activation.³³ In the context of tumor-derived antigens, cDC1s can serve as an autonomous platform for priming both CD4 and CD8 T cells.³⁴ In response to inflammation, circulating monocytes infiltrate the TME and upregulate CD11c, and major histocompatibility complex class II (MHCII). These monocyte-derived cells (MC) can be difficult to distinguish from cDC2s due to their expression of CD11b, CD172a, and IRF-4.³¹

Three clusters (C1–C3) were identified within the tumor-infiltrating DC population (figure 3A). C1 and C3 shared gene signatures of both cDC1 and cDC2 but differed in the expression of proliferation genes, which was enriched in C3 (figure 3B and online supplemental figure S3D). C2 lacked the conventional gene signatures associated with cDC1 and cDC2, but resembled recently described tumor-infiltrating ‘activated’ DCs that upregulate the expression of maturation and migration genes (*Fscn1*, *Ccr7*, *Il12b*, *Stat4*, *Tnfrsf9*) upon uptake of tumor antigens and secrete IL-12 in response to IFN-γ^{30–35–36} (figure 3B,C and online supplemental figure S3E). CCL21-DC ISV as monotherapy and in combination with anti-PD-1 led to the enrichment of this ‘activated’ DC cluster, which was annotated as mregDC (figure 3C). While all treatments resulted in a decrease in the tumor-infiltrating cDC population, as determined by both flow cytometry and scRNA-seq (figure 3C,D and online supplemental figure S2A, figure S3F), a concurrent increase in CD103⁺cDC1 and cDC2 was observed in TdLN by flow cytometry (figure 3E), suggesting enhanced cDC migration to TdLN. Enrichment of antigen-experienced CD44⁺ CD4 and CD8 T cells was also observed following CCL21-DC ISV and combination

therapy in TdLN (figure 3G), possibly due to increased T cell activation in TdLN.

CCL21-DC ISV induces an early influx of endogenous cDCs and T cells into the TME and egress of cDC1s to TdLN

To gain a better understanding of the interplay between endogenous and vaccine DCs, the kinetics of DC trafficking was evaluated at earlier timepoints following ISV. Mice-bearing KPL-3M tumors were treated with vehicle control or CellTracker Red-labeled CCL21-DC or mock-transduced DC (mock-DC), and tumors and TdLN were harvested at 2 hours, 24 hours, and 48 hours for analysis by flow cytometry (figure 3G). CCL21-DC and mock-DC vaccines were approximately 20% of the total live tumor-infiltrating CD45⁺ leucocytes at 24 hours and 4% at 48 hours following ISV (figure 3H). While there was a precipitous decrease in the fraction of red-labeled DCs within the TME over time, only a small fraction (<10%) of these cells was observed in TdLN at 24 hours, consistent with a recent report showing the retention of IT-injected DCs within the tumor (figure 3I).³⁷ A time-dependent decrease in viable red-labeled DCs, determined by Fixable Zombie Dye staining, was observed after IT injection, suggesting that the decrement in the number of DC vaccines over time likely results from cell death rather than DC egress (online supplemental figure S3G).

Both CCL21-DC and mock-DC induced an influx of endogenous (non-red) CD4 and CD8 T cells into the tumor 24 hours after ISV, which was significantly higher than vehicle control (figure 3J). While the magnitude of CD8 T cell induction was similar between the two DC vaccine groups (mock-DC or CCL21-DC), CCL21-DC resulted in a two-fold higher induction of CD4 T cell infiltration at 24 hours compared with mock-DC (figure 3J). A higher induction of CD4 T cell tumor-infiltration compared with that of CD8 T cells in response to CCL21-DC ISV is consistent with prior in vitro and in vivo studies showing enhanced migration of CD4 T cells compared with CD8 T cells in response to CCL21.^{22–23} A more than two-fold induction of tumor-infiltration by endogenous (non-red) cDC1s and cDC2s was also observed at 24 hours following ISV with CCL21-DC compared with mock-DC and vehicle control (figure 3K). Both mock-DC and CCL21-DC ISV promoted a statistically significant, sustained migration of cDC1 to TdLN following therapy at 24 hours and 48 hours compared with vehicle control (figure 3L). The observation that CCL21-DC ISV induces an influx of endogenous cDC1 into the TME and promotes sustained cDC1 egress to the TdLN is consistent with a recent report that has identified endogenous cDC1s as critical immune mediators that prime tumor-specific T cell responses in TdLNs following BM-DC ISV.³⁷

The efficacy of ISV with CCL21-DC is dependent on T cell egress from TdLN

Murine studies have identified that sustained T cell-mediated antitumor responses following anti-PD-1 therapy are dependent on T cell trafficking from TdLN into the

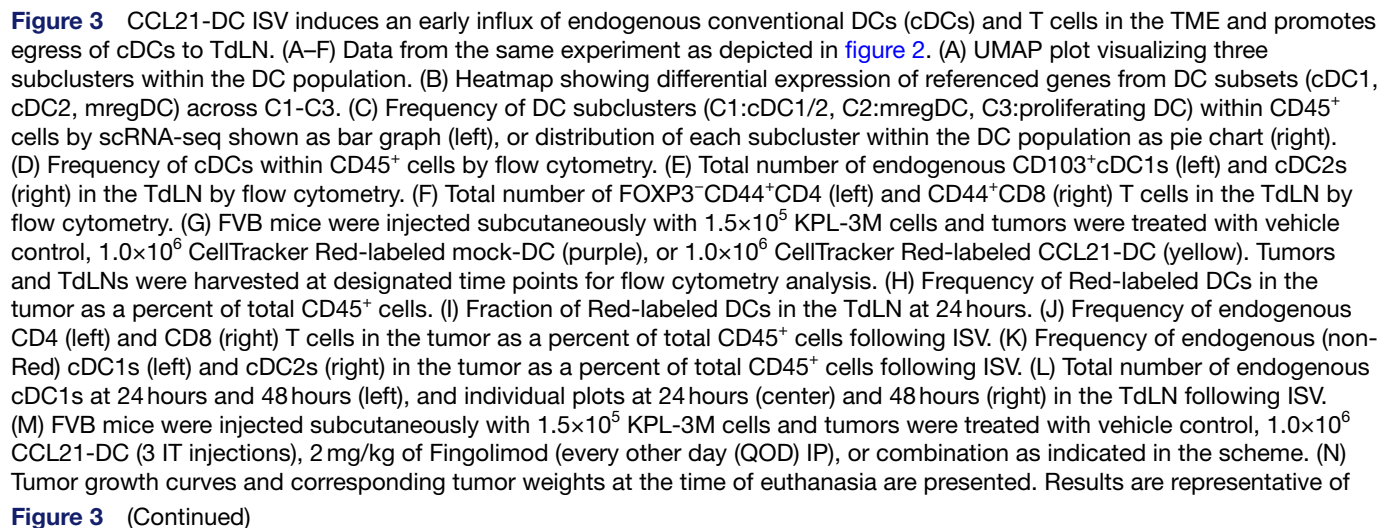


Figure 3 continued

two biological replicates of 6–10 mice per group. scRNA-seq was performed once. P values were determined by unpaired t-test. * $p < 0.05$, ** $p < 0.01$, *** $p < 0.001$, **** $p < 0.0001$. DC, dendritic cell; IP, intraperitoneal; ISV, in situ vaccination; IT, intratumoral; TdLN, tumor-draining lymph node; UMAP, Uniform Manifold Approximation and Projection.

tumor,^{38,39} yet it remains unknown whether continuous T cell trafficking between the tumor and TdLN is required for the antitumor efficacy of CCL21-DC ISV. KPL-3M tumor-bearing mice were treated with CCL21-DC in the presence or absence of fingolimod, which is a sphingosine-1 phosphate receptor modulator that sequesters lymphocytes in lymph nodes (figure 3M). Fingolimod monotherapy resulted in a modest reduction of KPL-3M tumor growth both in vivo and in vitro, consistent with prior reports documenting the direct tumor cytotoxicity of this drug (figure 3M and online supplemental figure S3H).⁴⁰ Addition of fingolimod to CCL21-DC reduced the antitumor efficacy to that of fingolimod alone, suggesting that activated T cells in TdLN are crucial mediators of CCL21-DC-induced antitumor responses.

CCL21-DC monotherapy and CCL21-DC/anti-PD-1 combination therapy induce the expansion of NK, Th1 and progenitor CD8 effector T cells in the TME

CCL21-DC monotherapy and CCL21-DC/anti-PD-1 combination therapy promoted infiltration of predominantly effector (CD62L⁺) FOXP3⁺CD4⁺ and CD8⁺ T cells and FOXP3⁺CD4⁺ regulatory T cells (Treg) into the TME as determined by flow cytometry (figure 4A and online supplemental figure S4A–D). scRNA-seq revealed four subclusters within CD4 effector T cells, with distinct gene signatures corresponding to T helper type 1 (Th1; C1), T helper type 2 (Th2; C4), dysfunctional CD4 T cells (Tdysfx; C3) expressing multiple exhaustion markers, including *Ctla4*, *Lag3*, *Pdcd1* and *Havcr2*, as well as central memory precursor CD4 T cells (Tcmp; C2) expressing *Tcf7* (encoding TCF-1) associated with increased memory stem cell potential⁴¹ (figure 4B,C). CCL21-DC alone or in combination with anti-PD-1 promoted significant expansion of the Th1 and Tcmp cells in the TME (figure 4D). Consistent with these results, FOXP3⁺CD4⁺ effector cells in the TME had increased expression of the activation marker PD-1 in response to CCL21-DC alone or in combination with anti-PD-1 as determined by flow cytometry, and these treatments resulted in a substantial reduction of exhausted FOXP3⁺CD4⁺ effector cells coexpressing PD1 and TIM3 (figure 4E). Enrichment of FOXP3⁺CD4⁺ effector cells in the TME following CCL21-DC alone and CCL21-DC/anti-PD-1 combination therapy was partially a result of increased proliferation, as evidenced by increased Ki-67 expression of this population (figure 4F). CCL21-DC monotherapy and CCL21-DC/anti-PD-1 combination also resulted in increased IFN- γ secretion from FOXP3⁺CD4⁺ effector cells, consistent with scRNA-seq data showing Th1 enrichment in the TME (figure 4G). The highest increase in FOXP3⁺CD4⁺ effector cell proliferation

and IFN- γ secretion was observed with combination therapy.

Clustering of tumor-infiltrating CD8 effector T cells, which were predominantly PD-1⁺, identified three clusters (C1–C3) (figure 4H and online supplemental figure S4E). C1 had low expression of effector genes but expressed memory gene signatures associated with self-renewal of the polyfunctional undifferentiated TILs that mediate the proliferative response to anti-PD-1 therapy^{42,43}; therefore, this cluster was designated as progenitor exhausted effector CD8 T cells (progenitor_exh) (figure 4I). C2 and C3 were annotated as terminally exhausted (terminally_exh) and effector like (effector_like) T cells based on their high expression of exhaustion and effector genes, respectively (figure 4I). CCL21-DC monotherapy and CCL21-DC/anti-PD-1 combination therapy resulted in the enrichment of CD8 effectors in the TME with an expansion of the progenitor_exh cells accompanied by a relative reduction of the terminally_exh subcluster within the CD8 effector compartment (figure 4J). This increase in tumor-infiltrating CD8 T cells following CCL21-DC ISV as monotherapy or in combination with anti-PD-1 is partially due to increased proliferation, indicated by higher Ki-67 expression in these cells which was highest in magnitude following combination therapy (figure 4K). Only combination therapy resulted in increased IFN- γ secretion by CD8 effector cells (figure 4L).

Cytotoxic natural killer (NK) cells are critical mediators of cancer surveillance that can autonomously eliminate tumor cells in an antigen-independent manner. CCL21-DC alone and CCL21-DC/anti-PD-1 combination therapy induced increased infiltration of endogenous NK cells in the TME with enhanced proliferation and IFN- γ secretion as determined by flow cytometry (figure 4M–O). An increased PD-L1 expression, as determined by mean fluorescent intensity, on tumors and MHC-II^{hi} M ϕ , MC, and cDC immune subtypes was observed following all therapies with the highest increase observed following combination therapy with CCL21-DC and anti-PD-1, possibly due to the enhanced IFN- γ production by NK and T cells in the TME (figure 4P).

CCL21-DC and CCL21-DC/anti-PD-1 promote sustained T cell infiltration and activation in the TME and induce systemic expansion of memory T cells

To assess the evolution of adaptive immune responses following ISV, immune phenotyping by flow cytometry was performed at a later time point on day 18, 12 days after the initiation of therapy (figure 5A and online supplemental figure S4F). An enrichment of CD45⁺ leucocytes was observed in the TME following CCL21-DC alone or

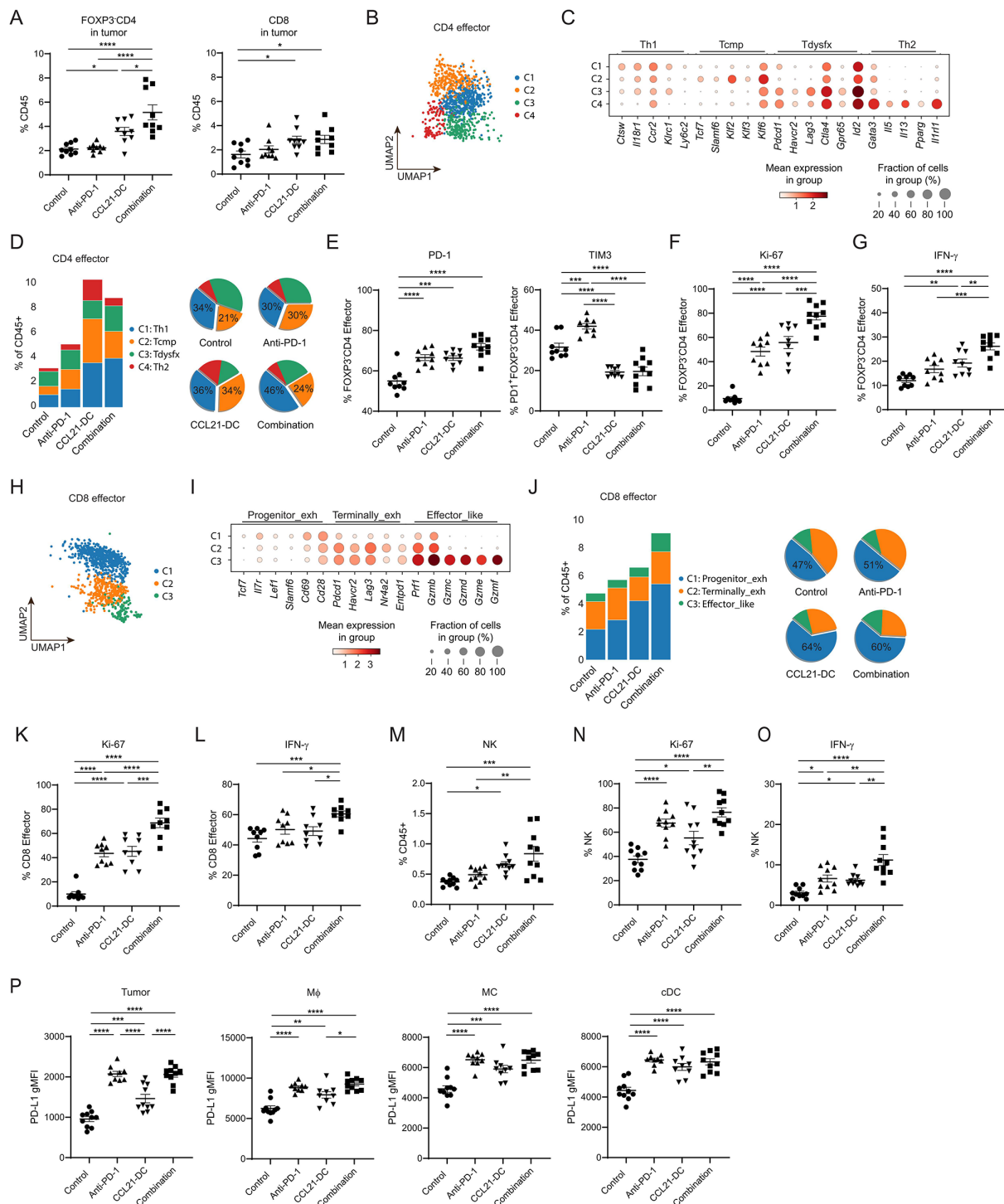


Figure 4 CCL21-DC ISV as monotherapy or in combination with anti-PD-1 induces NK and T cell infiltration, Th1 polarization, and expansion of progenitor T cells in the TME. Data from the same experiment depicted in figure 2. (A) Frequency of FOXP3⁺CD4⁺ (left) and CD8⁺ (right) T cells within CD45⁺ cells in the TME by flow cytometry. (B) UMAP plot visualizing four subclusters within the CD4 effector population. (C) Bubble plots showing the expression of sub-lineage markers (Th1, Th2, central memory precursor (Tcmp), and dysfunctional (Tdysfx) T cells) in individual clusters. The size of each circle is proportional to the percentage of cells expressing the gene and its intensity depicts the average transcript count within a cell. (D) Frequency of CD4 effector clusters (C1:Th1, C2:Tcmp, C3:Tdysfx, and C4:Th2) within CD4⁺ cells by scRNA-seq shown as bar graph (left), or distribution of each subcluster within CD4 effector cells as pie chart (right). (E) Percent of PD-1⁺ within FOXP3⁺CD4⁺ effectors (left) and TIM3⁺ among PD-1⁺ FOXP3⁺CD4⁺ effectors (right) in the TME by flow cytometry. (F) Ki-67 and (G) IFN- γ expression within FOXP3⁺CD4⁺ effector T cells in the TME by flow cytometry. (H) UMAP plot visualizing three subclusters within the CD8 effector population. (I) Bubble plots showing the expression of sub-lineage markers (progenitor_exh, terminally_exh, and effector (effector_like) T cells) in individual clusters as in (C). (J) Frequency of CD8

Figure 4 (Continued)

Figure 4 continued

effector clusters (C1: progenitor_exh, C2: terminally_exh, and C3: effector_like) within CD45⁺ cells by scRNA-seq shown as bar graph (left), or distribution of each subcluster within CD8 effectors as pie chart (right). (K) Ki-67 and (L) IFN- γ expression in CD8 effector T cells in the TME by flow cytometry. (M) Frequency of NK cells within CD45⁺ cells by flow cytometry. (N) Ki-67 and (O) IFN- γ expression in NK cells in the TME by flow cytometry. (P) Geometric MFI of PD-L1 on tumor cells, macrophages (M ϕ), monocyte-derived (MC), and cDC as determined by flow cytometry. Flow cytometry results are representative of two biological replicates of 6–10 mice per group. scRNA-seq was performed once. P values were determined by unpaired t-test. * $p < 0.05$, ** $p < 0.01$, *** $p < 0.001$, **** $p < 0.0001$. DC, dendritic cell; ISV, in situ vaccination; TME, tumor microenvironment; MFI, mean fluorescent intensity; UMAP, Uniform Manifold Approximation and Projection.

in combination with anti-PD-1, compared with control or anti-PD-1 monotherapy (online supplemental figure S4G). While a decrease in tumor-infiltrating FOXP3⁺ CD4 and CD8 T cells were observed on day 18 compared with day 15 in control mice, CCL21-DC promoted a persistent

enrichment of TILs in the TME on day 18 compared with anti-PD-1 and control, and addition of anti-PD-1 to CCL21 resulted in the highest increase of tumor T cell infiltration (figure 5B). Effector TILs from control mice had diminished IFN- γ production on day 18 compared

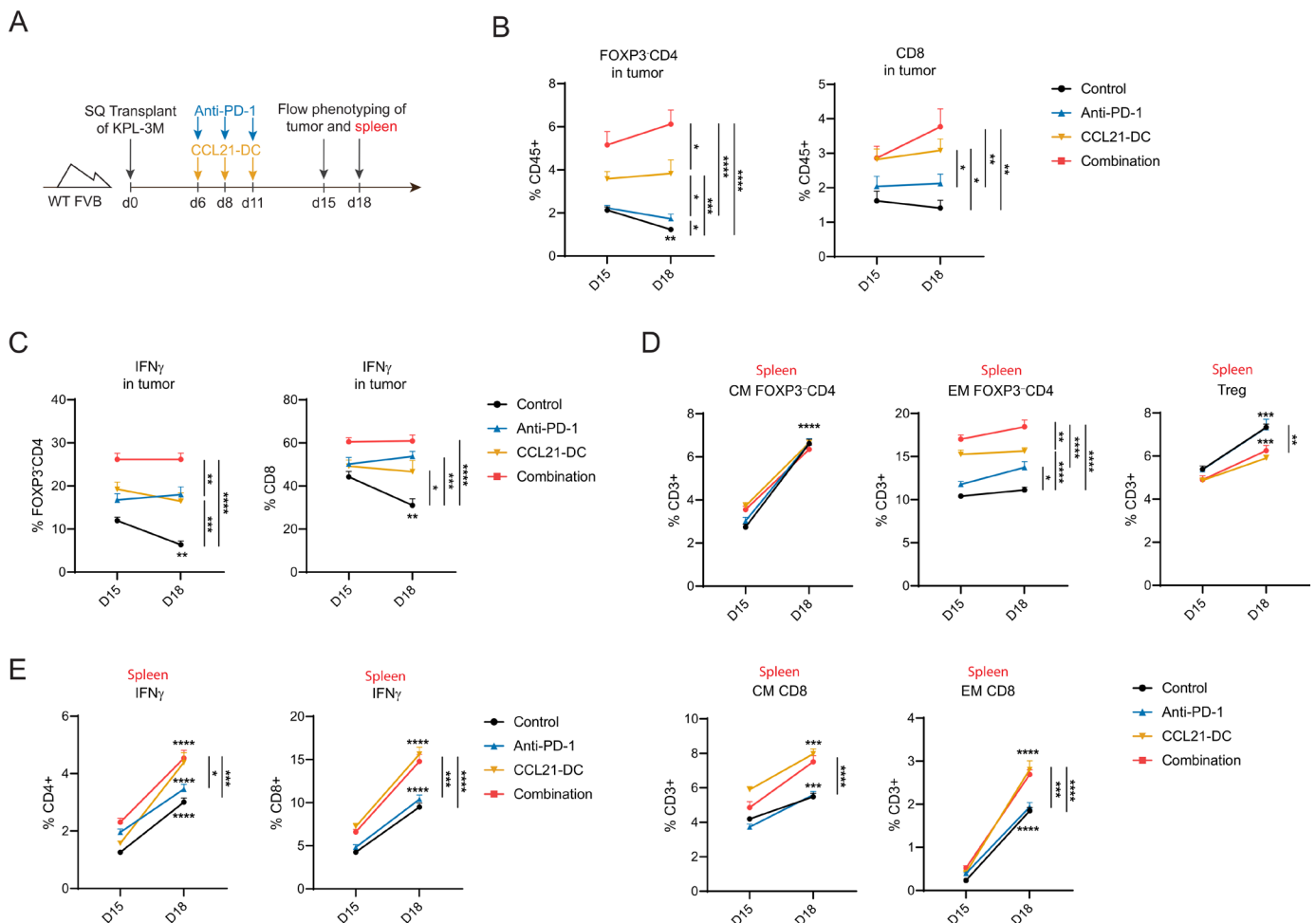


Figure 5 CCL21-DC ISV in combination with anti-PD-1 induces systemic expansion of memory T cells. (A) FVB mice were injected subcutaneously with 1.5×10^5 KPL-3M cells on day 0 and tumors were treated with vehicle control, 1.0×10^6 CCL21-DC (3 IT injections), 200 μ g of anti-PD-1 (3 IP injections), or combination as indicated in the scheme. Tumor and spleen were harvested on day 15 and day 18 for immunophenotyping by flow cytometry (n=6–10 per group). (B) Frequency of FOXP3⁺CD4 (left) and CD8 (right) T cells within CD45⁺ cells in the TME on day 15 and day 18. (C) IFN- γ expression in FOXP3⁺CD4 (left) and CD8 (right) T cells in the TME on day 15 and day 18. (D) Frequency of central memory (CM) FOXP3⁺CD4 (top-left), effector memory (EM) FOXP3⁺CD4 (top-middle), Treg (top-right), CM CD8 (bottom-left), and EM CD8 (bottom-middle) in CD3 cells in the spleen on day 15 and day 18. (E) IFN- γ expression in CD4 (left) and CD8 (right) T cells in the spleen on day 15 and day 18. Flow cytometry results are representative of two biological replicates of 6–10 mice per group. Statistics comparing temporal differences within the same group from day 15 to day 18 is shown above the day 18 data on the graph. Statistical analyses among treatment groups on day 18 is shown on the right side of the graph. P values were determined by unpaired t-test. * $p < 0.05$, ** $p < 0.01$, *** $p < 0.001$, **** $p < 0.0001$. DC, dendritic cell; IP, intraperitoneal; ISV, in situ vaccination; IT, intratumoral; TdLN, tumor-draining lymph node; TME, tumor microenvironment;.

with day 15, but CCL21-DC and anti-PD-1 alone or in combination sustained the production of IFN- γ in TILs (figure 5C). The addition of anti-PD-1 to CCL21-DC resulted in a statistically significant increase in the IFN- γ -producing effector FOXP3⁺CD4⁺ TILs compared with CCL21-DC monotherapy. These data illustrate that CCL21-DC ISV induces durable infiltration of CD4 and CD8 effectors in the TME and the combination with anti-PD-1 further augments tumor infiltration and effector function of these lymphocytes.

Lymphocytes from the spleen of tumor-bearing mice on day 15 and day 18 were evaluated by flow cytometry to determine systemic immune responses following therapy (figure 5A). For all treatments, temporal T cell expansion was observed in CD62L⁺CD44⁺ central memory (CM) FOXP3⁺CD4⁺ and CD8 T cells, CD62L⁺CD44⁺ effector memory (EM) CD8 T cells, as well as Tregs over time (day 18 compared with day 15) (figure 5D). There was no expansion in EMFOXP3⁺CD4⁺ T cells. Comparison of T cell subset frequencies among treatment groups revealed that CCL21-DC and combination therapy induced the expansion of CM CD8 T cells and EM FOXP3⁺CD4⁺ and CD8 T cells, but not CM FOXP3⁺CD4⁺ T cells, when compared with control and anti-PD-1 groups (figure 5D). CCL21-DC and combination therapy also led to a statistically significant decrease in splenic Tregs on day 18 compared with anti-PD-1 and control (figure 5D). Increased IFN- γ secretion from splenic CD4 and CD8 T cells was observed on day 18 compared with day 15, which was highest following CCL21-DC and combination therapy (figure 5E). These data suggest that CCL21-DC ISV as monotherapy or in combination with anti-PD-1 results in the expansion and activation of systemic T cells.

CCL21-DC/anti-PD-1 combination therapy promotes immunoediting of tumor subclones and generates systemic tumor-specific immune memory

The dynamic interplay between antigen-specific T cells and tumor cells can result in immunoediting of tumor cells and the escape of resistant clones.⁴⁴ We hypothesized that CCL21-DC ISV combined with anti-PD-1 could broaden functional antitumor T cell responses to induce immunoediting of tumor subclones. This was evaluated by whole exome sequencing (WES) of subcutaneous KPL-3M tumors (flow-sorted Live/CD45⁺ population), which are composed of a heterogeneous pool of tumor clones.²⁶ WES was performed on day 7 prior to initiation of therapy and at day 25 following treatment with vehicle control or CCL21-DC/anti-PD-1 combination therapy (figure 6A). Given that the combination therapy eradicated a significant fraction of subcutaneous tumors in this model, only stabilized or growing tumors were sequenced. Clustering of the mutation profiles of KPL-3M tumors based on variant allele frequency (VAF) revealed seven dominant mutation groups, corresponding to tumor subclones (figure 6B). The combination treatment eradicated C2 and C3 and facilitated the elimination of C4. No changes in C5 and C6 was noted following treatment, suggesting

that these clusters may be resistant to immune clearance. Emergence of C7 at day 25 may represent an enrichment of immune-resistant tumor subclone after tumor engraftment. These data provide evidence that CCL21-DC and anti-PD-1 combination therapy promotes immunoediting of tumor subclones, indicative of dynamic changes in the tumor-specific T cell repertoires in response to therapy.

To determine whether successful combination therapy could lead to the establishment of systemic tumor-specific immune memory, mice cured of KPL-3M tumors following combination therapy were re-challenged with KPL-3M or the control MyC-CaP tumor cells from the same FVB background 90 days post-treatment (figure 6C,D). After an initial tumor growth, cured mice rejected all KPL-3M tumors but succumbed to MyC-CaP tumors. Naive FVB mice served as additional controls and succumbed to both KPL-3M and MyC-CaP tumors. These data demonstrate the generation of systemic tumor-specific immune memory following successful eradication of KPL-3M tumors by CCL21-DC ISV and anti-PD-1 combination therapy.

DISCUSSION

Although ICI has led to improved survival in a subset of patients with NSCLC, the majority of patients do not respond and many develop resistance. One of the dominant prerequisites for response to ICI is T lymphocyte effector tumor infiltration, which is often absent at baseline or severely hindered by the immunosuppressive milieu of the TME.^{2,9,17} We found in this study that CCL21-DC ISV induces antitumor T cell responses and sensitizes multiple immune-refractory murine NSCLC models to anti-PD-1 therapy. We determined that CCL21-DC ISV combined with anti-PD-1 facilitates immunoediting of tumor subclones and establishes tumor-specific immune memory in preclinical models of NSCLC with increased TMB and clonal heterogeneity, indicating successful restoration of the cancer-immunity cycle¹⁷ and generation of sustained antitumor T cell responses. This study provides a rationale for clinical translation of this combination immunotherapy.

The immunosuppressive milieu of the TME in solid tumors is a formidable obstacle for the success of systemic immunotherapies, including ICI, adoptive T cell therapies and extra-tumoral delivery of cancer vaccines. Using a syngeneic murine model of LKB1-deficient NSCLC, we found that CCL21-DC ISV reprograms the immune compartment of the TME to facilitate endogenous antitumor T cell responses. Loss of LKB1 in NSCLC is a genomic driver of resistance to ICI and has been associated with a neutrophil-enriched TME with a paucity of T cells.^{27,29} scRNA-seq of the TME of LKB1-deficient tumors demonstrated that CCL21-DC ISV diminished tumor-promoting neutrophils and increased antitumor neutrophils with a type I IFN signature (figure 2). In accordance with these findings, CCL21-DC ISV was previously shown to result in a reduction of immunosuppressive molecules

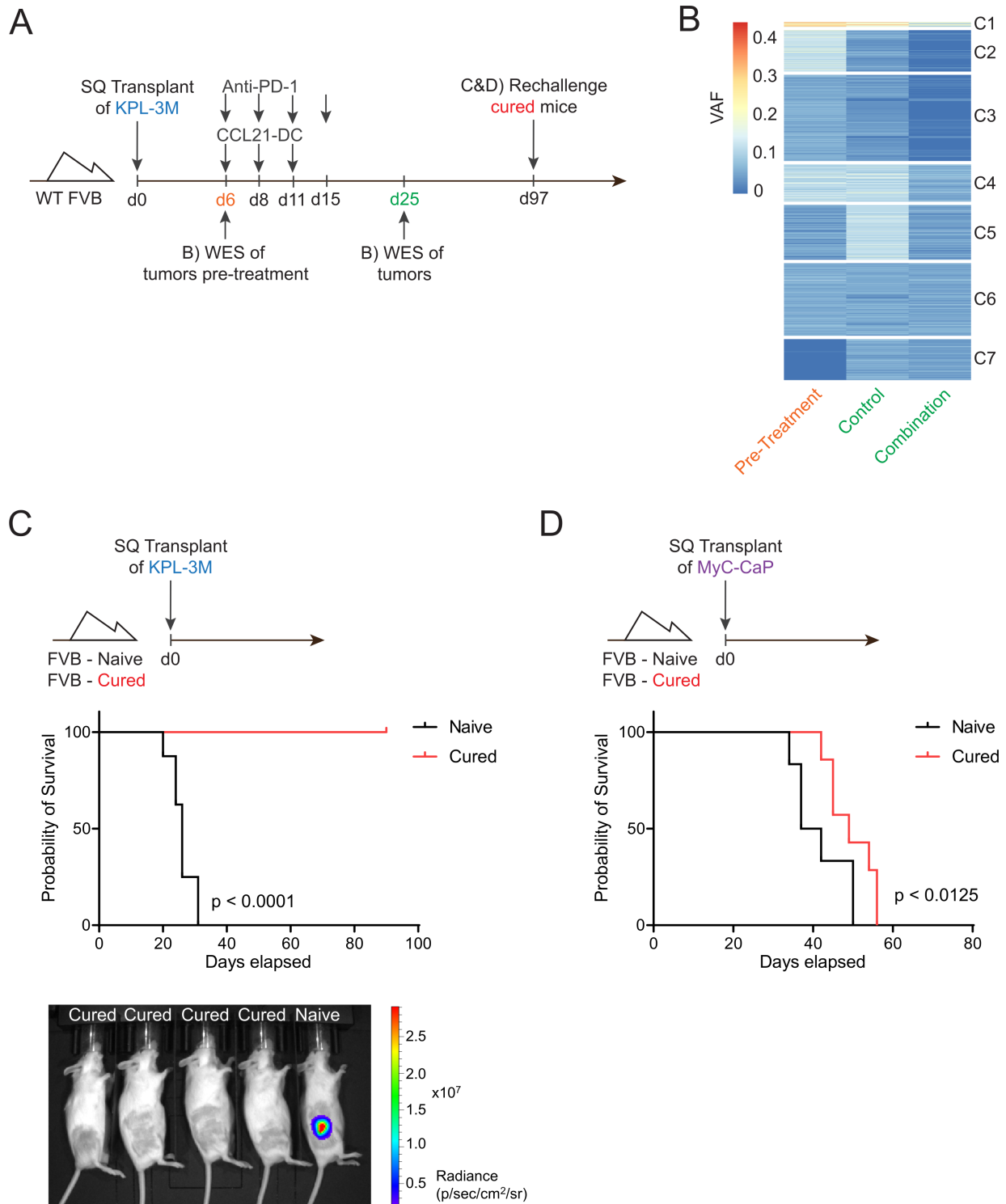


Figure 6 CCL21-DC ISV combined with anti-PD-1 promotes immunoediting of tumor subclones and generates systemic tumor-specific immune memory. (A) FVB mice were injected subcutaneously with 1.5×10^5 KPL-3M cells on day 0 and tumors were treated with vehicle control, or combination therapy with 1.0×10^6 CCL21-DC and $200 \mu\text{g}$ of anti-PD-1 as indicated in the scheme. Tumors were harvested on day 6 (prior to treatment) and day 25, flow sorted for CD45⁺ population and subjected to whole exome sequencing (WES). (B) Clustering of the mutational profiles of tumor cells based on variant allele frequency (VAF) revealed seven subclones. Combination therapy resulted in the elimination of C2 and C3, and near complete eradication of C1 and C4. (C) KPL-3M tumor-bearing FVB mice cured following combination therapy with CCL21-DC and anti-PD-1 (shown in figure 6A in red) were inoculated with 3.0×10^5 KPL-3M cells and tumor growth was assessed serially by bioluminescence imaging. Naïve FVB mice served as control. Bioluminescence images from day 10 and the survival plots are presented. (D) Same as (C) except that mice were inoculated with 2.0×10^6 syngeneic MyC-CaP cells. WES was performed once (three mice for pretreatment group on day 6 and four mice per group on day 25). Rechallenge studies are representative of three biological replicates of 6–8 mice per group. Statistical analysis was performed with log-rank test. DC, dendritic cell; ISV, in situ vaccination

in the TME associated with protumor neutrophils, including IL-10 and PGE2, and a concurrent induction of IFN-inducible chemokines, such as CXCL9 and CXCL10.²² Tumor-promoting neutrophils have emerged as potent immunosuppressive mediators that are negatively correlated with T cell tumor infiltration in NSCLC⁴⁵ and are associated with worse outcomes in patients with NSCLC treated with ICI.^{46,47} Our studies suggest that antitumor responses following the combination therapy of CCL21-DC ISV and anti-PD-1 could partially result from the alteration of the neutrophil compartment within the TME.

Tumor-residing cDCs are critical mediators of sustained antitumor T cell responses.^{19,39} The presence of tumor-infiltrating DC-LAMP⁺ mature DCs, a component of tertiary lymphoid structures, has been implicated as a positive prognostic indicator in patients with NSCLC.^{48,49} We show that in mice bearing LKB1-deficient NSCLC, the IT viability of DC vaccines was limited to 48 hours; however, CCL21-DC ISV induced a significant influx of endogenous cDC1s and cDC2s into the tumor at 24 hours after treatment, compared with control and mock-DC (figure 3). These data are consistent with prior studies demonstrating the superior antitumor efficacy of CCL21-DC as compared with mock-DC²² and underscore the utility of cytokine engineering of DC vaccines to condition the TME. Using scRNA-seq, we observed a significant enrichment of activated mregDCs within the DC compartment of the TME, with the highest magnitude observed following the CCL21-DC ISV anti-PD-1 combination therapy. Recent studies show that mregDCs are a rare population of DC-LAMP⁺ tumor-residing DCs in NSCLC with high expression of IL-12,^{36,50} an essential cytokine for CD4 Th1 polarization and CD8 T cell activation.¹⁹ This finding aligns with our previous study demonstrating increased concentration of IL-12 and IFN- γ within the TME of murine tumors following CCL21-DC ISV.²² In accordance with these findings, we show that CCL21-DC ISV induces sustained infiltration of CD4 and CD8 T lymphocytes, Th1 polarization, and the expansion of progenitor/precursor T cells within the TME (figure 4). Cognate antigen-specific Th1 licensing of DCs is required for the generation of effective CD8 T responses.³³ The addition of PD-1 blockade to CCL21-DC ISV enhanced the expansion of local and systemic CD4 and CD8 T cells with improved IFN γ production, consistent with the synergistic efficacy of the combination therapy in this murine model.

A prior study using lymphotaxin knockout mice (LT $\alpha^{-/-}$), which lack peripheral lymph nodes, demonstrated the presence of IFN γ -secreting TILs following CCL21-DC ISV, suggesting the possibility of extranodal T cell priming.²³ Our immunophenotyping data revealed that in addition to inducing an initial influx of endogenous cDCs into the tumor, CCL21-DC ISV facilitated sustained cDC1 trafficking to TdLNs. These data, combined with the observation that the antitumor efficacy of CCL21-DC

ISV was dependent on T cell egress from TdLNs, suggest that T cell activation in response to CCL21-DC ISV likely occurs in TdLN rather than the TME in this murine model. Consistent with this premise, a recent study³⁷ used *Irf8+32^{-/-}* mice, which lack endogenous cDC1, to demonstrate that ISV with BM-DCs requires endogenous cDC1 for T cell activation. Our studies highlight the complex interaction between endogenous and vaccine DCs that support antitumor responses following CCL21-DC ISV.

In contrast to antigen-based vaccines, DC ISV bypasses the need for the cumbersome and imprecise process of patient-specific antigen identification and can potentially generate a broad T cell response against a diverse repertoire of epitopes present in solid tumors. We have previously shown that CCL21-DC ISV monotherapy induced de novo systemic T cell responses against known tumor-associated antigens, as determined by ELISPOT, in approximately 40% of the patients with advanced NSCLC in a phase 1 trial.²⁵ We found that CCL21-DC ISV plus anti-PD-1 induces the elimination of multiple tumor subclones in a syngeneic murine model of LKB1-deficient NSCLC, suggesting that this combination therapy can broaden the endogenous pool of functional tumor-specific T cells. Immunoediting as an in vivo readout of T cell function is a more translationally relevant approach compared with the assessment of T cell proliferation and cytokine secretion employed in murine models expressing highly immunogenic epitopes, such as ovalbumin. Our studies indicate that successful tumor immunoediting and rejection did not require activation or antigen-loading of CCL21-DC prior to IT injection, consistent with other reports.^{22,23,37} This finding is in contrast to studies using extratumoral administration of DC vaccines which require activation and antigen-loading prior to delivery.¹⁹ Our immunoediting studies in combination with tumor rechallenge experiments in cured mice (figure 6) demonstrate that combination of CCL21-DC ISV with anti-PD-1 can generate effective antitumor T cell responses that provide immunological memory.

The results reported here should be viewed in the context of the limitations of the study. First, subcutaneous murine tumor models lack the latency of tumorigenesis and do not fully recapitulate the complex immunopathological microenvironment of human NSCLC. However, subcutaneous tumors allow for normalization of tumor sizes prior to treatment and are readily accessible for multiple IT injections of DC vaccine. Second, the early initiation of combination immunotherapy, necessitated by rapid kinetics of tumor growth in syngeneic models, differs from the clinical application of this therapy in advanced-stage NSCLC. Future immune monitoring studies using biospecimens from patients with advanced NSCLC enrolled in an ongoing phase 1 clinical trial of IT CCL21-DC in combination with pembrolizumab are necessary to validate our results and identify immune signatures associated with improved clinical outcomes.

In summary, we found that CCL21-DC ISV can overcome resistance to immunotherapy in murine NSCLC. In the context of LKB1-deficient NSCLC with increased TMB, the combination of CCL21-DC ISV and anti-PD-1 ameliorates the immunosuppressive TME and induces long-lasting systemic tumor-specific T cell immunity. On the basis of these preclinical findings and the previously established feasibility and safety of CCL21-DC ISV monotherapy in patients with advanced NSCLC, an ongoing phase 1 clinical trial is evaluating the safety and efficacy of CCL21-DC ISV plus pembrolizumab in patients with advanced NSCLC refractory to front-line therapy.

METHODS

Study design

We evaluated the antitumor efficacy of ISV with CCL21-DC as an approach to overcome resistance to immunotherapy in NSCLC. We used syngeneic murine models of NSCLC with known driver mutations and varying mutational burden. Treatments included CCL21-DC and anti-PD-1, as monotherapies or in combination, as well as corresponding vehicle or isotype controls. Statistical analysis and the numbers of mice per group are discussed in detail in statistical methods and figure legends. To ensure consistent tumor sizes, outlier tumors, as determined by Grubbs' test, were removed prior to randomization of mice to treatment groups. To minimize potential confounders, mice from different treatment groups were randomly distributed in cages. In vivo experiments are representative of at least two replicates unless otherwise stated in figure legends. In vitro experiments used biological triplicates and data are representative of at least two replicates.

Cell lines

The murine cell line 1940A was established from lung adenocarcinomas of conditional *Kras*^{G12D}*Tp53*^{+/-}*Lkb1*^{-/-}*Luc* (KPL) FVB mice that express firefly luciferase.²⁶ WES analysis revealed that KPL cells lost the other allele of *Tp53* upon in vitro culture and, therefore, bear a *Kras*^{G12D}*Tp53*^{-/-}*Lkb1*^{-/-}*Luc* genotype.²⁶ The *Kras*^{G12D} LKR-13 line, established from a lung adenocarcinoma tumor from a *K-ras*^{LA1} mouse, was generously provided by Dr. Jonathan Kurie.²⁶ The KPL-3M cell line with increased mutational burden was generated by in vitro exposure a KPL cell line to N-methyl-N-nitrosourea as previously described.²⁶ MyC-CaP cell line was purchased from the American Type Culture Collection. All cell lines were maintained in complete culture media (RPMI-1640 with L-glutamine (Corning) supplemented with 10% FBS (Gemini) and 1% penicillin/streptomycin (Fisher Scientific)) at 37°C in a humidified atmosphere of 5% CO₂ and used before 5 passages. Cell lines were periodically tested for authentication and routinely confirmed to be free of *mycoplasma* contamination (Lonza Mycoalert).

Syngeneic tumor studies

FVB/N mice and 129-E mice were purchased from Charles River Laboratories. Tumor cells were implanted in mice aged 7–9 weeks subcutaneously at optimal doses as indicated in figure legends. Tumor length and width were measured blindly by caliper and the volume calculated by the equation: $0.4 \times \text{length} \times \text{width}^2$. For immunotherapy studies, mice bearing ~50 mm³ tumors were randomized and treated with control, IT CCL21-DC (1×10^6 cells), IP 200 µg of anti-PD-1 antibody (BioXcell, Clone RMP1-14) or combination as illustrated in the figures. IP administration of rat IgG2a (BioXcell, Clone 2A3) was used as an isotype control for anti-PD-1. For T cell egress studies, FVB/N mice bearing KPL-3M tumors were treated with fingolimod (2 mg/kg) every other day starting at day 5, 1 day prior to treatment of tumors with IT CCL21-DC (1×10^6 cells). For secondary tumor challenge studies, mice were euthanized when tumor volume reached 1500 mm³. In vivo bioluminescence images were obtained by IVIS Spectrum imager 10 min after IP injection of D-luciferin (150 mg/kg). For DC trafficking studies, mock-DCs and CCL21-DCs were labeled with CellTracker Red CMTPX (Invitrogen) fluorescent dye per manufacturer's protocol prior to IT injection.

In vitro tumor cell proliferation in response to fingolimod

KPL-3M cells were plated in culture media in 96-well plates at 1000 cells per well in 6 replicates and treated with fingolimod at various concentrations as indicated in the figure. Proliferation was measured using ATPlite 1 step Luminescence Assay Kit (Perkin Elmer) every 24 hours up to 96 hours. Readings at each time point were normalized to the reading at baseline to control for plating differences.

Generation of CCL21-DC

BMDCs were generated as previously described.²² Briefly, BM cells were cultured in DC media (RPMI-1640+10% FBS) with 20 ng/mL murine GM-CSF (Pepro-tech) and 10 ng/mL murine IL-4 (Pepro-tech). The cells (2.5×10^6 cells/mL) were seeded into a sterile non-tissue culture-treated six-well plastic plate at 2 mL per well in a humidified CO₂ incubator (37°C, 5% CO₂). On day 3, media was changed with fresh DC media containing GM-CSF and IL-4. On day 6, loosely adherent and floating cells were harvested and washed with DPBS. Cells were resuspended into pHIV-CCL21 (construction detailed in online supplemental material) and virus media and plated at 3 mL per well (1×10^6 cells/mL) into a new non-tissue culture-treated six-well plastic plate and spininfected at 800×g for 2 hours at 32°C. Following transduction, cells were collected and washed twice with DPBS prior to injection. CCL21-DCs phenotype was characterized by flow cytometry and viability was assessed by Trypan-blue (Gibco) staining before and after lentiviral transduction for all experiments. DC antigen-uptake and CCL21

production was quantified by FITC Dextran and ELISA, respectively, as described in online supplemental material.

Murine tumor, spleen, and lymph node processing

Single-cell suspensions of murine tumors and spleens were prepared as previously described.²⁶ Briefly, murine tumors were minced and digested in complete culture media containing 1 mg/mL of Collagenase IV (Roche) and 50 unit/mL DNase (Sigma) at 37°C with shaking every 10 min. After 30 min of incubation, 10 mL of fresh complete culture media was added and the samples were filtered through a 70 µm filter and centrifuged. Red blood cells were lysed on ice for 5 min with red blood cell lysis solution (BioLegend) followed by addition of complete media. Spleens and lymph nodes were mashed through a 70 µm filter and centrifuged. Red blood cells were lysed as described above, and the cells were washed with PBS, and counted.

Flow cytometry

Single-cell suspensions of in vitro generated DCs or murine tumors, spleens and lymph nodes were incubated with antibodies for 20 min at 4°C, followed by washing with staining buffer (DPBS+2% FBS). Surface staining and intracellular staining for FOXP3 and Ki-67 were performed as previously described.²⁶ IFN γ production was evaluated by intracellular staining after in vitro stimulation with Cell Stimulation Cocktail (eBioscience) for 4 hours, using the intracellular fixation and permeabilization buffer set (eBioscience). Data acquisition was performed on Attune NxT (ThermoFisher) or Novo-Cyte Quanteon (Agilent) cytometer, and data analyzed by FlowJo software (TreeStar). Antibodies are detailed in online supplemental table S1.

scRNA-seq and data analysis

Single-cell suspensions from tumors were stained with Zombie-NIR LIVE/DEAD stain and CD45 antibody for 20 min at 4°C. Viable leucocytes were sorted using BD Biosciences Aria II cell sorter with 100 µm nozzle. The 10X Genomics platform (10X Genomics, Pleasanton, CA) was used for single-cell transcriptomic analysis. Single-cell encapsulation, library construction, and sequencing were performed at the UCLA Technology Center for Genomics and Bioinformatics (TCGB) core facility. Libraries were prepared according to the Chromium Single Cell 3' Reagent Kit v3 (10X Genomics) user guide and sequencing was performed on the NovaSeq 6000 (Illumina). 10X Cell Ranger (V.3.1.0) software was used to align reads to the mouse genome mm10 and to generate gene count matrices using the Ensemble transcript reference (V.93). Poor quality and doublet cells were removed based on either detected genes (<200 or >9000 genes), total UMIs (<1000 or >100 000 counts), or percentage of reads aligned to mitochondrial genome (>20%). In total, 18 170 cells (from 4 treatment arms) passed quality control for analysis. Scanpy package (V.1.6.0)

was used to normalize, scale and select high variance gene features and to perform dimensional reduction and differential gene expression analyses. Briefly, principal component (PCs) analysis was applied using the expressions of the top 4000 highest variable genes and the first 50 PCs were selected for Uniform Manifold Approximation and Projection visualization and cell clustering using the Louvain algorithm. T-test approach was used to identify cluster marker genes (sc.tl.rank_genes_groups function with t-test_overestim_var method) and differential gene expression associated with treatments (sp.stats.ttest_ind function).

Genomic profiling

Genomic profiling of tumor cells was performed as previously described.²⁶ Briefly, genomic DNA was extracted from tumor cells by DNeasy Blood and Tissue Kit (Qiagen). DNA extracted from two tails of FVB mice was included as a normal reference for variant calls. DNA libraries were prepared using the Kapa Hyper Prep Kit (Roche) followed by exome enrichment with SeqCap EZ Share Developer Probe (Roche). Sequencing was performed on HiSeq3000 instrument as 150 bp pair-end runs with the aim of 100× depth at UCLA TCGB Core facility. Raw reads were aligned to the mouse genome (mm10) with Burrows-Wheeler Aligner (V.0.7.17), then marked for duplicates and recalibrated as suggested by Genome Analysis Toolkit (GATK). Strelka2 was used to call variants between tumor and individual normal genome independently. A variant was called a mutation if it was (1) called by both comparisons to different normal genomes, (2) not in the germline mutation panel derived from the FVB, (3) not supported by any read in the associated normal genomes, and (4) detected by at least five reads in tumors with VAF>0.1. Ensembl Variant Effect Predictor was used to annotate passed variants for missense and nonsense mutations. Tumors from three mice on day 6 (pretreatment group) and 4 mice per group (control or combination) on day 25 were subjected to WES analysis. A mutation was defined as stabilized if it was called in at least two tumors in a specific experimental group. The associated VAF was defined by the average of individual tumors.

Statistical analysis and reproducibility

Experiments were performed at least twice unless otherwise indicated. Results from one representative experiment are shown. Statistical analyses were performed in Prism (V.9) software (GraphPad) unless otherwise noted; a $p<0.05$ was considered statistically significant. Results are reported as mean \pm SEM unless otherwise indicated. For tumor growth studies, flow phenotyping, cytokine production and gene expression, differences between groups were evaluated by two-tailed unpaired t-tests. To determine synergism, differences between observed and predicted mathematical outcomes were evaluated by two-tailed unpaired t-test. For mouse survival studies, differences between groups were evaluated by log-rank test.

Author affiliations

¹Medicine, David Geffen School of Medicine at UCLA, Los Angeles, CA, USA

²Medicine, VA Greater Los Angeles Healthcare System, Los Angeles, CA, USA

³Molecular and Medical Pharmacology, David Geffen School of Medicine at UCLA, Los Angeles, CA, USA

⁴Medicine, Zhejiang University School of Medicine, Hangzhou, Zhejiang, People's Republic of China

⁵Pathology and Laboratory Medicine, David Geffen School of Medicine at UCLA, Los Angeles, California, USA

Acknowledgements The authors thank Lauren Winter and Elvira Licican for administrative support. We acknowledge the UCLA Technology Center for Genomics and Bioinformatics for WES and scRNA-seq support and the UCLA Jonsson Comprehensive Cancer Center (JCCC) Flow Cytometry Core for assistance with cell sorting.

Contributors Conceptualization: SMD, RS-R and BL. Experimental planning: RS-R, RJL, YD, LMT, RL, CD, SJP, CS, AEL and EBG. Investigation: RS-R, RJL, RL, SLO, ZLH, CD, SJP, WC, BK, JA, MS and MP. Data and research analysis: RS-R, RJL, YD, LMT, RL, SLO, ZLH, CD, TZ, SJP, WC, BK, JA, CS, MO, MS, MP and KK. Supervision: SMD, BL and EBG. Writing: RS-R, BL, SMD, KK and EBG. Guarantor: SMD, RS-R, and BL.

Funding This study was supported in part by funding from: National Cancer Institute 1U01-CA196408 (SMD). National Institute of Health/National Center for Advancing Translational Sciences UL1TR001881 (SMD). Medical Research Funds from the Department of Veterans Affairs (RSR, SMD). National Heart Lung and Blood Institute T32-HL072752 (RSR). Lung Cancer Foundation of America and International Lung Cancer Foundation Young Investigator Award (RSR). Tobacco-Related Disease Research Program Predoctoral Fellowship Award (RJL). The UCLA Jonsson Comprehensive Cancer Center Research Flow Cytometry Core is supported by the National Institutes of Health P30 CA-16042 and 5P30 AI-28697.

Competing interests SMD is an advisory board member for EarlyDiagnostics, T-Cure Bioscience, LungLife AI, and previously served as an advisor to Johnson and Johnson Lung Cancer Initiative. SMD has received research funding from Johnson and Johnson Lung Cancer Initiative and Novartis. EBG has an advisory role for Abbvie; ABL-Bio; AstraZeneca; Boehringer-Ingelheim; Bristol Myers Squibb; Dracen Pharmaceuticals; EMD Serono; Eisai; Eli Lilly; Gilead; GlaxoSmithKline; Ipsen; Merck; Natera; Novartis; Personalis; Regeneron; Sanofi; Shionogi; and Xilio Therapeutics. EBG receives research support from ABL Bio; AstraZeneca; Bristol Myers Squibb; Daiichi Sankyo; Dynavax Technologies; Eli Lilly; EMD Serono; Genentech; Iovance Biotherapeutics; Merck; Mirati Therapeutics; Neon; and Novartis. AEL is an advisory board member for AstraZeneca, Bristol Myers Squibb, Leica Biosystems, Jazz Pharmaceuticals, Novocure, Pfizer, MorphoSys, Eli Lilly, Oncocyte, Novartis, Regeneron, Janssen oncology, Sanofi group of companies. AEL receives research support from Daiichi Sankyo, Calithera Biosciences, AstraZeneca, Dracen Pharmaceuticals, WindMIL, eFFECTOR Therapeutics. AEL has an immediate family member employed by Boston Scientific with stock (<5% equity).

Patient consent for publication Not applicable.

Ethics approval Mice were housed in pathogen-free facilities at University of California, Los Angeles (UCLA) and all procedures were approved by the UCLA Animal Research Committee (ARC-2017-049).

Provenance and peer review Not commissioned; externally peer reviewed.

Data availability statement All data relevant to the study are included in the article or uploaded as online supplemental information. All data associated with this study are present in the main text or the online supplemental materials. pHIV-dTomato was obtained through a material transfer agreement (MTA) with Addgene. Gene expression data (accession number PRJNA916837) are available at www.ncbi.nlm.nih.gov/geo/. Plasmids and cell lines used in this study have not been deposited to any repositories. These materials are available on request.

Supplemental material This content has been supplied by the author(s). It has not been vetted by BMJ Publishing Group Limited (BMJ) and may not have been peer-reviewed. Any opinions or recommendations discussed are solely those of the author(s) and are not endorsed by BMJ. BMJ disclaims all liability and responsibility arising from any reliance placed on the content. Where the content includes any translated material, BMJ does not warrant the accuracy and reliability of the translations (including but not limited to local regulations, clinical guidelines, terminology, drug names and drug dosages), and is not responsible for any error and/or omissions arising from translation and adaptation or otherwise.

Open access This is an open access article distributed in accordance with the Creative Commons Attribution Non Commercial (CC BY-NC 4.0) license, which

permits others to distribute, remix, adapt, build upon this work non-commercially, and license their derivative works on different terms, provided the original work is properly cited, appropriate credit is given, any changes made indicated, and the use is non-commercial. See <http://creativecommons.org/licenses/by-nc/4.0/>.

ORCID iDs

Ramin Salehi-Rad <http://orcid.org/0000-0003-1543-5421>

Rui Li <http://orcid.org/0000-0002-5620-4833>

Manash Paul <http://orcid.org/0000-0002-9404-0024>

Edward B Garon <http://orcid.org/0000-0001-7077-8801>

REFERENCES

- 1 Siegel RL, Miller KD, Fuchs HE, et al. Cancer statistics, 2021. *CA Cancer J Clin* 2021;71:7–33.
- 2 Salehi-Rad R, Li R, Paul MK, et al. The biology of lung cancer: development of more effective methods for prevention, diagnosis, and treatment. *Clin Chest Med* 2020;41:25–38.
- 3 Gandhi L, Rodríguez-Abreu D, Gadgeel S, et al. Pembrolizumab plus chemotherapy in metastatic non-small-cell lung cancer. *N Engl J Med* 2018;378:2078–92.
- 4 Borghaei H, Paz-Ares L, Horn L, et al. Nivolumab versus Docetaxel in advanced squamous non-small-cell lung cancer. *N Engl J Med* 2015;373:1627–39.
- 4 Borghaei H, Paz-Ares L, Horn L, et al. Nivolumab versus Docetaxel in advanced squamous-cell non-small-cell lung cancer. *N Engl J Med* 2015;373:1627–39.
- 6 Sharma P, Hu-Lieskovan S, Wargo JA, et al. Primary, adaptive, and acquired resistance to cancer immunotherapy. *Cell* 2017;168:707–23.
- 7 Herbst RS, Soria J-C, Kowanetz M, et al. Predictive correlates of response to the anti-PD-L1 antibody Mpd3280A in cancer patients. *Nature* 2014;515:563–7.
- 8 Rizvi NA, Hellmann MD, Snyder A, et al. Cancer Immunology. mutational landscape determines sensitivity to PD-1 blockade in non-small cell lung cancer. *Science* 2015;348:124–8.
- 9 Tumeh PC, Harview CL, Yearley JH, et al. PD-1 blockade induces responses by inhibiting adaptive immune resistance. *Nature* 2014;515:568–71.
- 10 Garon EB, Rizvi NA, Hui R, et al. Pembrolizumab for the treatment of non-small-cell lung cancer. *N Engl J Med* 2015;372:2018–28.
- 11 McGranahan N, Furness AJS, Rosenthal R, et al. Clonal neoantigens elicit T cell immunoreactivity and sensitivity to immune Checkpoint blockade. *Science* 2016;351:1463–9.
- 12 Gettinger SN, Choi J, Mani N, et al. A dormant TIL phenotype defines non-small cell lung Carcinomas sensitive to immune Checkpoint blockers. *Nat Commun* 2018;9:3196.
- 13 Ayers M, Luceford J, Nebozhyn M, et al. IFN-gamma-related mRNA profile predicts clinical response to PD-1 blockade. *J Clin Invest* 2017;127:2930–40.
- 14 Litchfield K, Reading JL, Puttick C, et al. Meta-analysis of Tumor- and T cell-intrinsic mechanisms of sensitization to Checkpoint inhibition. *Cell* 2021;184:596–614.
- 15 McGranahan N, Rosenthal R, Hiley CT, et al. Allele-specific HLA loss and immune escape in lung cancer evolution. *Cell* 2017;171:1259–71.
- 16 Cummings AL, Gukasyan J, Lu HY, et al. Mutational landscape influences Immunotherapy outcomes among patients with non-small-cell lung cancer with human Leukocyte antigen Supertype B44. *Nat Cancer* 2020;1:1167–75.
- 17 Chen DS, Mellman I. Elements of cancer immunity and the cancer-immune set point. *Nature* 2017;541:321–30.
- 18 Champiat S, Tselikas L, Farhane S, et al. Intratumoral Immunotherapy: from trial design to clinical practice. *Clin Cancer Res* 2021;27:665–79.
- 19 Wculek SK, Cueto FJ, Mujal AM, et al. Dendritic cells in cancer Immunology and Immunotherapy. *Nat Rev Immunol* 2020;20:7–24.
- 20 Adamik J, Butterfield LH. What's next for cancer vaccines. *Sci Transl Med* 2022;14:eabo4632.
- 21 Sharma S, Yang S-C, Hillinger S, et al. SLC/Ccl21-mediated anti-tumor responses require Ifngamma, MIG/Cxcl9 and IP-10/Cxcl10. *Mol Cancer* 2003;2:22.
- 22 Yang S-C, Hillinger S, Riedl K, et al. Intratumoral administration of Dendritic cells overexpressing Ccl21 generates systemic antitumor responses and confers tumor immunity. *Clin Cancer Res* 2004;10:2891–901.
- 23 Kirk CJ, Hartigan-O'Connor D, Mulé JJ. The Dynamics of the T-cell antitumor response: Chemokine-Secreting Dendritic cells can prime tumor-reactive T cells Extranodally. *Cancer Res* 2001;61:8794–802.

- 24 Sharma S, Zhu L, Srivastava MK, *et al.* Ccl21 Chemokine therapy for lung cancer. *Int Trends Immun* 2013;1:10–5.
- 25 Lee JM, Lee M-H, Garon E, *et al.* Phase I trial of Intratumoral injection of Ccl21 gene-modified Dendritic cells in lung cancer elicits tumor-specific immune responses and Cd8(+) T-cell infiltration. *Clin Cancer Res* 2017;23:4556–68.
- 26 Salehi-Rad R, Li R, Tran LM, *et al.* Novel Kras-mutant murine models of non-small cell lung cancer possessing Co-occurring Oncogenic mutations and increased tumor mutational burden. *Cancer Immunol Immunother* 2021;70:2389–400.
- 27 Skoulidis F, Goldberg ME, Greenawalt DM, *et al.* Stk11/Lkb1 mutations and PD-1 inhibitor resistance in KRAS-mutant lung adenocarcinoma. *Cancer Discov* 2018;8:822–35.
- 28 Chung W-J, Daemen A, Cheng JH, *et al.* Kras mutant genetically engineered Mouse models of human cancers are Genomically heterogeneous. *Proc Natl Acad Sci U S A* 2017;114:E10947–55.
- 29 Li R, Salehi-Rad R, Crosson W, *et al.* Inhibition of granulocytic myeloid-derived Suppressor cells overcomes resistance to immune Checkpoint inhibition in Lkb1-deficient non-small cell lung cancer. *Cancer Res* 2021;81:3295–308.
- 30 Zilionis R, Engblom C, Pfirsche C, *et al.* Single-cell Transcriptomics of human and Mouse lung cancers reveals conserved myeloid populations across individuals and species. *Immunity* 2019;50:1317–34.
- 31 Bosteels C, Neyt K, Vanheerswynghe M, *et al.* Inflammatory type 2 cDCs acquire features of Cdc1S and Macrophages to Orchestrate immunity to respiratory virus infection. *Immunity* 2020;52:1039–56.
- 32 Gerhard GM, Bill R, Messemaker M, *et al.* Tumor-infiltrating Dendritic cell States are conserved across solid human cancers. *J Exp Med* 2021;218:e20200264.
- 33 Murphy TL, Murphy KM. Dendritic cells in cancer Immunology. *Cell Mol Immunol* 2022;19:3–13.
- 34 Ferris ST, Durai V, Wu R, *et al.* Cdc1 prime and are licensed by Cd4(+) T cells to induce anti-tumour immunity. *Nature* 2020;584:624–9.
- 35 Garriss CS, Arlauckas SP, Kohler RH, *et al.* Successful anti-PD-1 cancer Immunotherapy requires T cell-Dendritic cell Crosstalk involving the Cytokines IFN- γ and IL-12. *Immunity* 2018;49:1148–61.
- 36 Maier B, Leader AM, Chen ST, *et al.* A conserved Dendritic-cell regulatory program limits Antitumour immunity. *Nature* 2020;582:E17:257–62.
- 37 Ferris ST, Ohara RA, Ou F, *et al.* Cdc1 vaccines drive tumor rejection by direct presentation independently of host Cdc1. *Cancer Immunol Res* 2022;10:920–31.
- 38 Fransen MF, Schoonderwoerd M, Knopf P, *et al.* Tumor-draining lymph nodes are pivotal in PD-1/PD-L1 Checkpoint therapy. *JCI Insight* 2018;3:e124507.
- 39 Spranger S, Dai D, Horton B, *et al.* Tumor-residing Batf3 Dendritic cells are required for Effector T cell trafficking and adoptive T cell therapy. *Cancer Cell* 2017;31:711–23.
- 40 Rupp T, Debasly S, Genest L, *et al.* Therapeutic potential of Fingolimod and dimethyl fumarate in non-small cell lung cancer Preclinical models. *Int J Mol Sci* 2022;23:8192.
- 41 Ciucci T, Vacchio MS, Gao Y, *et al.* The emergence and functional fitness of memory Cd4⁺ T cells require the transcription factor Thpok. *Immunity* 2019;50:91–105.
- 42 Miller BC, Sen DR, Al Abosy R, *et al.* Subsets of exhausted Cd8(+) T cells Differentially mediate tumor control and respond to Checkpoint blockade. *Nat Immunol* 2019;20:326–36.
- 43 Siddiqui I, Schaeuble K, Chennupati V, *et al.* Intratumoral Tcf1(+)PD-1(+)Cd8(+) T cells with stem-like properties promote tumor control in response to vaccination and Checkpoint blockade Immunotherapy. *Immunity* 2019;50:195–211.
- 44 Mittal D, Gubin MM, Schreiber RD, *et al.* New insights into cancer Immunoediting and its three component phases--elimination, equilibrium and escape. *Curr Opin Immunol* 2014;27:16–25.
- 45 Kargl J, Busch SE, Yang GHY, *et al.* Neutrophils dominate the immune cell composition in non-small cell lung cancer. *Nat Commun* 2017;8:14381.
- 46 Kargl J, Zhu X, Zhang H, *et al.* Neutrophil content predicts lymphocyte depletion and anti-Pd1 treatment failure in NSCLC. *JCI Insight* 2019;4:e130850.
- 47 Schalper KA, Carleton M, Zhou M, *et al.* Elevated serum Interleukin-8 is associated with enhanced Intratumor neutrophils and reduced clinical benefit of immune-Checkpoint inhibitors. *Nat Med* 2020;26:688–92.
- 48 Dieu-Nosjean M-C, Antoine M, Danel C, *et al.* Long-term survival for patients with non-small-cell lung cancer with Intratumoral Lymphoid structures. *J Clin Oncol* 2008;26:4410–7.
- 49 Goc J, Germain C, Vo-Bourgais TKD, *et al.* Dendritic cells in tumor-associated tertiary Lymphoid structures signal a Th1 cytotoxic immune Contexture and license the positive Prognostic value of infiltrating Cd8+ T cells. *Cancer Res* 2014;74:705–15.
- 50 Leader AM, Grout JA, Maier BB, *et al.* Single-cell analysis of human non-small cell lung cancer lesions refines tumor classification and patient stratification. *Cancer Cell* 2021;39:1594–609.